“BABEŞ-BOLYAI” UNIVERSITY OF CLUJ-NAPOCA
FACULTY OF CHEMISTRY AND CHEMICAL ENGINEERING
INORGANIC CHEMISTRY DEPARTMENT

Amalia-Zorica HRISTEA-SIMOC (married MESAROŞ)

“OXIDE MATERIALS WITH SPECIAL OPTICAL PROPERTIES”

PhD Thesis Abstract

JURY PRESIDENT:

Associate professor dr. **CORNELIA MAJDIK** –dean

SCIENTIFIC ADVISOR:

Prof. dr. **IONEL HAIDUC**

REVIEWERS:

C. P. I, dr. **MARIA ZAHARESCU**

“I. G. Murgulescu” Institute of Physical-Chemistry, Bucharest

C. P. I, dr. **ELISABETH-JEANNE POPOVICI**

“Raluca Ripan” Institute for Research in Chemistry, UBB, Cluj - Napoca

Prof. dr. **TRAIAN PETRIŞOR**

Technical University, Cluj-Napoca

CONTENT

Keywords: luminescent materials, yttrium tantalate, thin films, laser ablation, chemical solution deposition

Abstract

The aim of this thesis is the synthesis of oxide materials based on yttrium tantalate as powders and thin films with luminescent properties. The thesis presents the influence of synthesis parameters on the crystalline structure, morphology and luminescent characteristics of $YTaO_4$, $YTaO_4$:Nb, $YTaO_4$:Nb/RE (RE: Eu, Tb) powders. The oxide materials samples were prepared by the solid-state reaction route. Low dimensional $YTaO_4$:Nb thin films were deposited by pulsed laser deposition and chemical solution deposition method. X-ray diffraction, FT-IR spectroscopy, scanning electron microscopy, transmission electron microscopy, atomic force microscopy and fluorescence spectroscopy analysis were used to investigate the crystalline structure, morphology and optical properties of both powders and thin films. The results were published in four articles.

INTRODUCTION

The researches undertaken within this thesis contribute to the widening of knowledge by the approach of a challenging field of interest, namely that of yttrium tantalate host lattice powders and thin films with luminescent properties. The studies performed within the thesis envisage the elucidation of several new aspects regarding the luminescent material based on orthotantalate host lattice.

- *self-activated $YTaO_4$,*
- *activated with niobium ions, $YTaO_4$:Nb,*
- *activated with niobium and rare earths (RE – Rare Earth), $YTaO_4$:Nb/RE.*

Under these circumstances, the influence of the preparative factors, such as: calcination temperature, the nature of mineralizing agents, the concentration of the activator ion in the host lattice on the structural, morphological and luminescent characteristics of the powders have been taken into consideration. Thus, several physical and chemical aspects regarding the effect of the mineralizing agent on the formation of the oxide lattice and on the activator incorporation degree have been considered. The investigation methods used for the study of the synthetized materials have been: X-ray diffraction, IR spectroscopy, optical microscopy, scanning electronic microscopy and luminescence spectroscopy. The studies performed on the powder oxide material envisage applicative aspect regarding the double correlation composition (synthesis conditions)-structure-properties.

The research carried out for the synthesis and the characterization of the niobium activated yttrium tantalate, $YTaO_4$:Nb thin films presents a fundamental character, since-until now-the scientific literature does not present any information regarding this topic.

The thin films preparation methods performed in the frame of this thesis have been: laser ablation and chemical solution deposition, while the structural characteristics have been determined by X-ray diffraction, the morphological ones by scanning electronic microscopy and atomic force microscopy. The optical-luminescent properties of the as-obtained thin films have been determined by luminescence spectroscopy.

The thesis is divided into two main parts: „Literature study regarding oxide materials with luminescent properties" and „Original contributions to the synthesis oxide powders and thin films with luminescent properties, to which the introduction and the general conclusions were added. The material is structured on six chapters, having a list of reference at the end of each chapter.

The first part gathers the scientific literature information regarding the luminescence of crystalline inorganic compounds, the synthesis and characterization of oxide materials-powders and thin films-with luminescent properties, being divided into three chapters:

- *Chapter 1* – is focused on the luminescence of inorganic substances with respect to the luminescence phenomenon and on the applicative potential of these materials;
- *Chapter 2* – is dedicated to a revision of the main synthesis methods and specific characterization methods both for oxide powders and thin films with pre-requisite properties;
- *Chapter 3* – gathers scientific literature information regarding the synthesis and the characterization of yttrium tantalate host lattice material;

The second part comprises the original scientific contributions regarding the preparation and the characterization of the oxide powders and thin films with yttrium tantalate host lattice $YTaO_4$, being structured on three chapters, as follows:

- *Chapter 4* – describes the experimental procedure used for the $YTaO_4$, $YTaO_4$:Nb and $YTaO_4$:Nb/RE powder preparation by solid state reactions and the investigation methods used for their characterization;
- *Chapter 5* – illustrates the investigation results on $YTaO_4$, $YTaO_4$:Nb and $YTaO_4$:Nb/RE powders with respect to the influence of various preparative factors on the structural, morphological and optical properties;
- *Chapter 6* – is dedicated to the study and characterization of $YTaO_4$:Nb thin films obtained both by a physical-laser ablation and chemical method-chemical solution deposition.

The thesis ends with the final conclusions comprising a synthesis of the obtained results. The originality of the paper results both from the studies carried out on oxide powders with $YTaO_4$ host lattice, and especially from the synthesis and characterization, for the first time, of the $YTaO_4$:Nb thin films.

It has to be mentioned that the presented results have been accomplished chronologically at the Raluca Ripan Institute for Research in Chemistry, Cluj-Napoca, Solid State Chemistry Group (CP

I dr. Elisabeth-Jeanne Popovici), ´ngstrom Laboratory within the University of Uppsala, Sweden, Materials Science Department (Prof. dr. Mats Boman) and the Materials Science Laboratory within the Technical University of Cluj-Napoca (Prof. Dr. Lelia Ciontea). The results presented in the thesis have been published, communicated or are under press.

I: LITERATURE STUDY:
OXIDE MATERIALS WITH LUMINESCENT PROPERTIES

CHAPTER 3: SYNTHESIS, CHARACTERISTCS AND PROPERTIES OF YTTRIUM TANTALATE LUMINESCENT MATERIALS

3.1. General aspects

Yttrium tantalates are a class of efficient roentgeno-luminescent materials used in medical imaging applications. These luminescent materials exhibit good X-ray absorbsion and emit in the ultraviolet-blue region of the electromagnetic spectrum. Their main applications regrd the manufacturing of different medical imaging detectors, such as: X-ray intensifying screens or scintillators – electronic systems – used in computed radiography or tomography. The role of these materials is to reduce the required X-ray dose to obtain anatomical details of the human body parts.

3.2. Synthesis methods

The synthesis of $YTaO_4$ luminescent materials class is usually achieved by the solid state reaction route. [1, 2, 15-26].

3.3. Structural and morphological characteristics

Yttrium tantalate powders present a complex polymorphism: [23, 28, 30-39]:

- low-temperature (1200^oC-1300^oC) – monoclinic structure (fergusonit);
- high temperature, up to 1400^oC – tetragonal structure (scheelit);
- under special conditions – temperature, flux – an additional monoclinic phase, designated as M-prime form (M'-$YTaO_4$)
- metastable structure T', obtained by the sol-gel method at temperatures below 850^0C – (fluorite).

Schematic, the $YTaO_4$ polymorphism can be illustrated by the following structural modifications [28, 34, 35]:

$$T' \xrightarrow{850^0 C} M' \xrightarrow{\approx 1325^0 C} T \xrightarrow{\text{Cooling}} M$$

(metastable phase)

The two monoclinic crystalline phases M and M' show different structural arrangements. In M'-$YTaO_4$ – figure 3.6 - tantalum atoms are situated in a distorted octahedral coordination with six Ta-O bonds (Ta-O: 4 short bonds 1.86-1.95 ´ and 2 bond: 2,23 ´), whereas in M-$YTaO_4$ tantalum is in tetrahedral coordination. Moreover, the unit cell volume of M' phase is approximately half of that of the M phase.

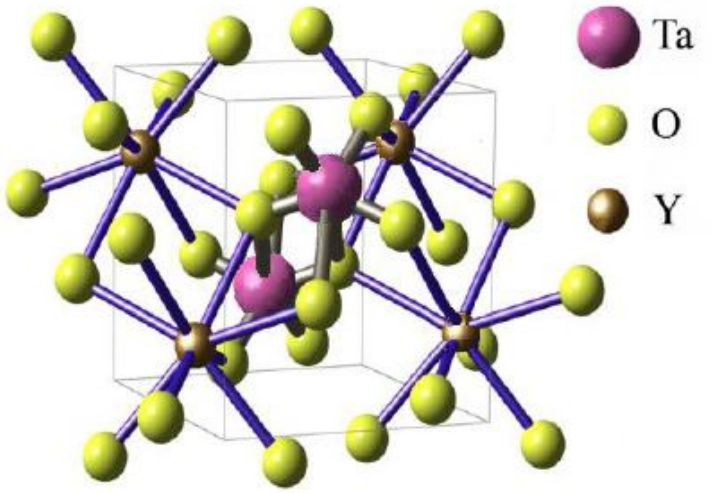

Figure 3.5. Monoclinic structure M'-$YTaO_4$ [40]

3.4. Luminescent properties

The high luminescence performances of niobium activated yttrium tantalate phosphor are associated with the monoclinic crystalline structure, M'-$YTaO_4$ representing the equilibrium phase at room temperature.

Yttrium tantalate polycrystalline with no activators can be excited with very short-wavelength ultraviolet (229 nm) radiation, cathode rays or X-rays. The photoluminescent emission spectrum consists in one more or less structured band peaking at about 335 nm. The luminescence is due to a charge-transfer transition into the tantalate group. For TaO_4, this charge-transfer transition requires

considerably higher energy than for NbO_4; this is the reason why $YTaO_4$ cannot be excited with 254 nm. The M' structure, where the average Ta-O distances are closer than those in the M structure, present a more efficient charge-transfer process, as well. If Nb is substituted for Ta in M'-$YTaO_4$, even more efficient emission is observed.

The luminescence emission could be shifted toward longer wavelengths when niobium is substituted for tantalum, or when rare earth ions, such as: Eu^{3+}, Tb^{3+}, Gd^{3+}, Sm^{3+}, Dy^{3+}, Pr^{3+} are used to replace the yttrium ions into the $YTaO_4$ structure [15, 48, 50-55].

II: ORIGINAL RESULTS ON THE SYNTHESIS OF OXIDE POWDERS AND THIN FILMS WITH LUMINESCENT PROPERTIES

CHAPTER 4: ORIGINAL INVESTIGATIONS ON THE SYNTHESIS OF YTTRIUM TANTALATE- BASED OXIDE POWDERS

4. 1. General aspects

The studies present several aspects regarding the synthesis of yttrium tantalate host matrix luminescent materials:

- *self-activated yttrium tantalate $YTaO_4$;*
- *niobium activated yttrium tantalate, $YTaO_4$:Nb,*
- *niobium and rare earth activated yttrium tantalate, $YTaO_4$:Nb/RE.*

The influence of activator concentration, thermal treatment schedule and flux nature on the crystalline structure, particle morphology and luminescent characteristics of $YTaO_4$: host lattice luminescent materials are investigated. The goal of these studies is to establish a correlation between the structural and morphological characteristics and optical properties in order to define the synthesis conditions that generate high performing luminescent materials.

4. 2. Oxide materials synthesis

Yttrium tantalate samples were prepared by solid state reaction – figure 4.1. The synthesis consists in the calcination of yttrium oxide and tantalum oxide as sources for the host matrix, niobium oxide, europium oxide or terbium oxide as sources for the activator ions, and lithium sulphate and/or

natrium sulphate as flux. The thermal treatment was achieved under different thermal conditions to ensure the formation of the host crystalline matrix and luminescent centers.

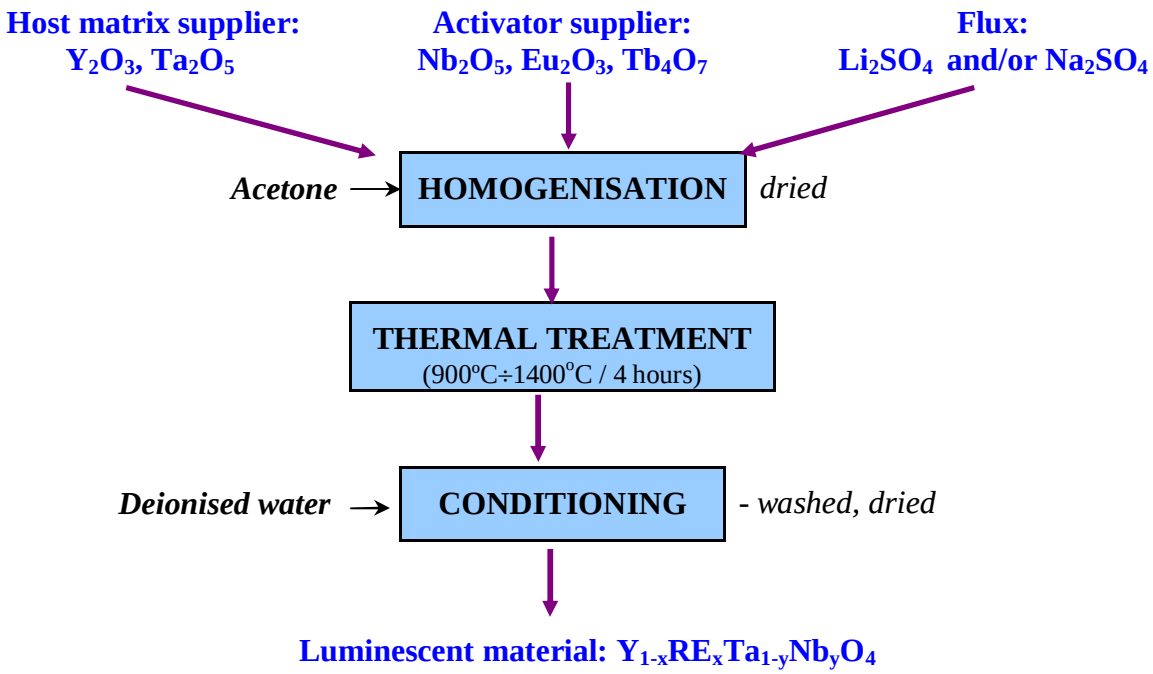

Figure 4.1.Yttrium tantalate host matrix solid state synthesis

Reaction mechanism

The formation of $YTaO_4$: Nb phosphors can be described by the equations

- ***$YTaO_4$***

$$Y_2O_3 + Ta_2O_5 + M_2SO_4 \rightarrow 2MTaO_3 + Y_2O_2SO_4 \quad (1)$$

$$2MTaO_3 + Y_2O_2SO_4 \rightarrow 2YTaO_4 + M_2SO_4 \quad (2)$$

- ***$YTaO_4$:Nb***

$$Y_2O_3 + (1-x)Ta_2O_5 + xNb_2O_5 + M_2SO_4 \rightarrow 2(1-x)MTaO_3 + 2xMNbO_3 + Y_2O_2SO_4 \quad (3)$$

$$2(1-x)MTaO_3 + 2xMNbO_3 + Y_2O_2SO_4 \rightarrow 2YTa_{1-x}Nb_xO_4 + M_2SO_4 \quad (4)$$

where: x = 0 ÷ 0.2

- ***$YTaO_4$:Nb/RE***

$$(1-x)Y_2O_3 + xRE_2O_3 + (1-y)Ta_2O_5 + yNb_2O_5 + M_2SO_4 \rightarrow$$

$$Y_{2(1-x)}RE_{2x}O_2SO_4 + 2(1-y)MTaO_3 + 2yMNbO_3 \quad (5)$$

$$Y_{2(1-x)}RE_{2x}O_2SO_4 + 2(1-y)MTaO_3 + 2yMNbO_3 \rightarrow 2Y_{1-x}RE_xTa_{1-y}Nb_yO_4 + M_2SO_4 \quad (6)$$

where: RE: Eu, Tb x = 0÷0.07 and M: Li, Na, y = 0.15

CHAPTER 5: THE INFLUENCE OF THE SYNTHESIS CONDITIONS ON THE STRUCTURAL, MORPHOLOGICAL AND LUMINESCENT PROPERTIES

The performed researches present some specific aspects on the synthesis of luminescent oxide materials based on yttrium tantalate. The goal is to establish a correlation between the morpho-structural and optical properties in order to define the synthesis conditions that generate a high performing luminescent material. The parameters influencing the synthesis are:

- *thermal treatment: temperature ($900^oC \div 1400^oC$), duration (2÷6 hours)*;
- *flux nature lithium sulphate and/or natrium sulphate;*
- *activator nature and concentration: Nb^{5+}, Nb^{5+} and Eu^{3+}, respectively Nb^{5+} and Tb^{3+}*

They define the conditions that generate a high performing luminescent material.

5.1. Self-activated yttrium tantalate, $YTaO_4$

5.1.1. Thermal treatment influence

The crystalline structure of yttrium tantalate was investigated by X-ray diffraction. The diffractograms for TA1-TA3, T19, T23 and T27 samples, thermally treated in the temperature range 900÷1400^{o}C with Li_2SO_4 flux addition are presented in figure 5.1. Comparative analysis of these diffractograms present the increase of the M'- $YTaO_4$ - (JCPDS PDF nr. 24-1425) reflexion lines and the decrease of the intermediate compounds, ($LiTaO_3$, $Y_2O_2SO_4$) reflexions, as well. The formation of T- $YTaO_4$ structure at higher temperature is in good agreement with the literature data.

5.1.2. Flux influence

Structural characteristics

The synthesis parameters and the structural, morphological and luminescent characteristics for the $YTaO_4$ samples are presented in table 5.2. The formation of M' crystalline phase can be observed by the structural analysis of T19-T21 samples – prepared with Li_2SO_4 and Li_2SO_4+Na_2SO_4 as flux - figure 5.7.

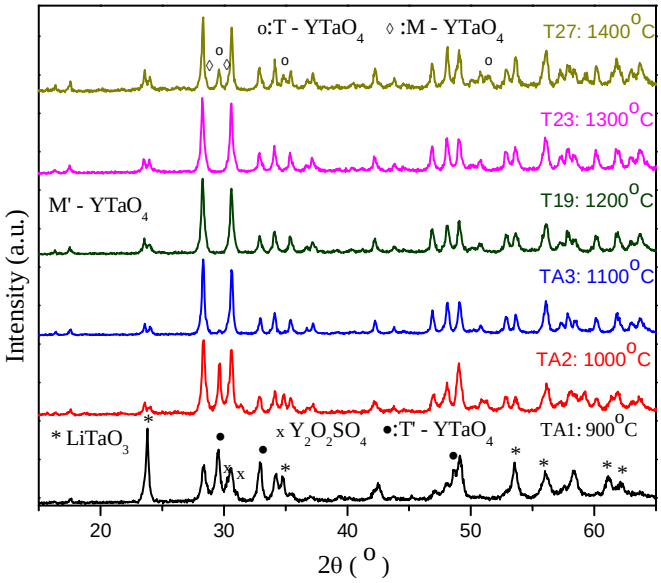

Figure 5.1. X-ray diffraction analysis of TA1-TA3, T19, T23, T27 samples

Table 5.2. The synthesis parameters and the structural, morphological and luminescent characteristics for the $YTaO_4$ samples

Sample	Synthesis conditions		Characteristics				
	Flux	Firing regime	Crystalline structure	$D_{crystallites}$ (nm)	$D_{particles}$ - L/l (μm)	Emission	
						I_{336}(a.u..)	λ(nm)
T19	Li_2SO_4	1200°C/4 h	M’	30	2-3 / 1-2	235	336
T20	Li_2SO_4:Na_2SO_4	1200°C/4 h	M’	32	4-5 / 1-2	260	338
T21	Na_2SO_4	1200°C/4 h	M’+T’	21	1-1.5	63	336
T23	Li_2SO_4	1300°C/4 h	M’	32	4-5 / 2-3	367	336
T24	Li_2SO_4:Na_2SO_4	1300°C/4 h	M’	31	4-5 / 2-3	249	338
T25	Na_2SO_4	1300°C/4 h	M’	28	2-2.5	270	336
T27	Li_2SO_4	1400°C/4 h	M’+T+M	43	11-12	215	339
T28	Li_2SO_4:Na_2SO_4	1400°C/4 h	M’+M	30	4-4.5	123	341
T29	Na_2SO_4	1400°C/4 h	M’+M	23	4-5	167	338

One can note that, in spite of the fact that Li_2SO_4, (m.p.= 884°C) and Na_2SO_4, (m.p.= 860°C) possess close melting point values, their behaviour as flux is very different due to the large difference between the two cation sizes. Lithium (Li^+= 0.073nm) which is a smaller cation with respect to sodium (Na^+= 0.113nm), is in the favour of the total conversion of oxides into the M’-$YTaO_4$ crystalline phase.

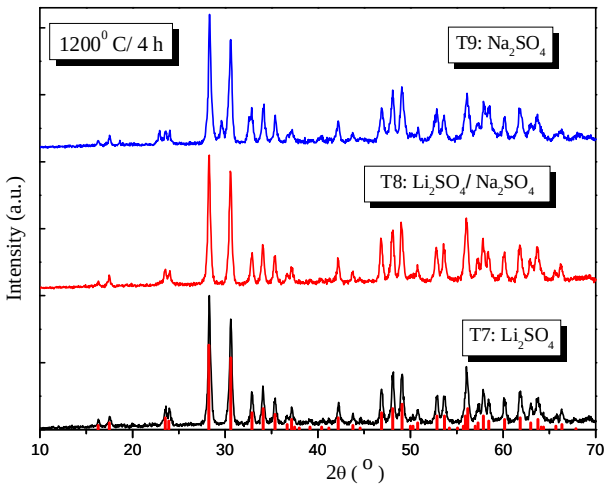

Figure 5.7. X-ray analysis of samples prepared at 1200°C

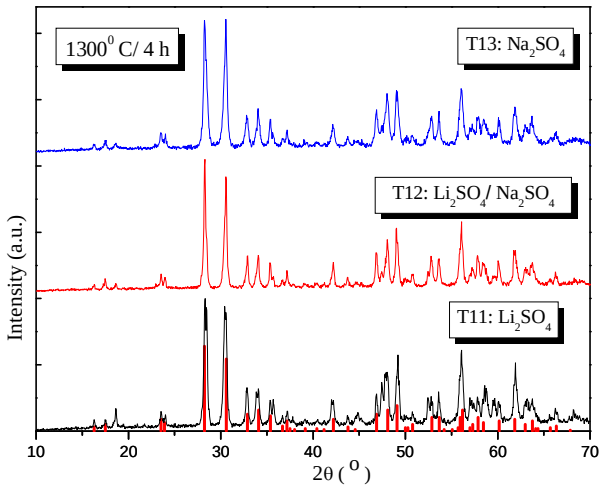

Figure 5.9. X-ray analysis of samples prepared at 1300°C

5.2. Niobium activated yttrium tantalate, $YTaO_4$:Nb

5.2.1. Optimum activator concentration

The crystalline structure and order degree of the phosphor samples were evaluated on the basis of *X-ray diffraction* patterns (XRD) and *FTIR spectra.*

Incorporation of up to about 15% niobium atoms into the yttrium tantalate host lattice determines the formation of $YTaO_4$ -$YNbO_4$ solid solutions - figure 5.18. Samples T1-T4 prepared with 0 ÷ 15 mole % niobium are single phase crystalline with M' phase structure. The sample T5 prepared with 20 mole % niobium ($YTa_{0.80}Nb_{0.20}O_4$) can be considered as double phase crystalline powder consisting of the niobium-rich M'-$YTaO_4$ phase and the tantalum-rich M-$YNbO_4$ phase. The yttrium niobate crystalline powder (sample T6) shows monoclinic M-phase structure.

The infrared spectra - figure 5.19 – stands for the idea that the crystalline host lattice of the powder with niobium concentration higher than 15% shows a low crystalline order degree, as compared with samples with 0-15 mol% Nb. The substitution of tantalum by niobium atoms preserves the M' crystalline structure, as already pointed out by X-ray diffraction, and influences mainly the bands observed at, $\nu_{s:}$ 812-806 cm^{-1}, 445-440 cm^{-1} and ν_{as}: 740-730 cm^{-1}, 660-620 cm^{-1}, bands assigned to degenerated ν(Ta-O) vibration modes and ν(Ta-O-Ta), respectively. The infrared spectra suggest a good incorporation of niobium ions into the host crystalline lattice of the T1-T4 samples, i.e. a relatively homogeneous distribution of the NbO_4^{3-} groups replacing the TaO_4^{3-} groups into the M'- $YTaO_4$ crystalline matrix.

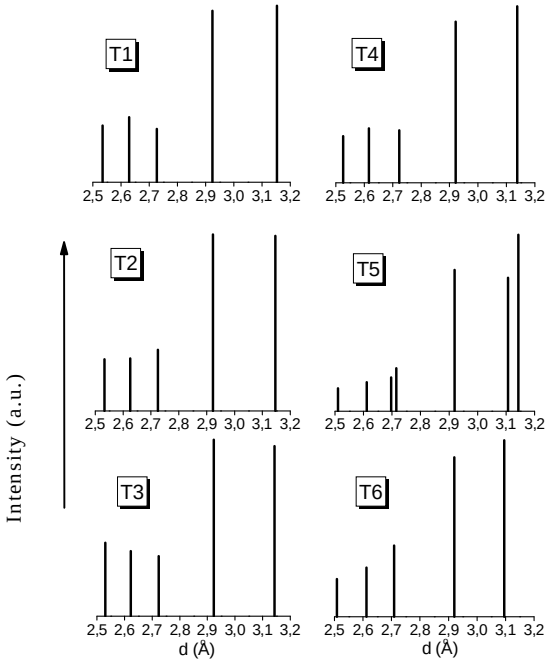

Figure 5.18. Position and relative intensity of the main diffraction lines of yttrium tantalate samples: T1-T5 and yttrium niobate sample - T6

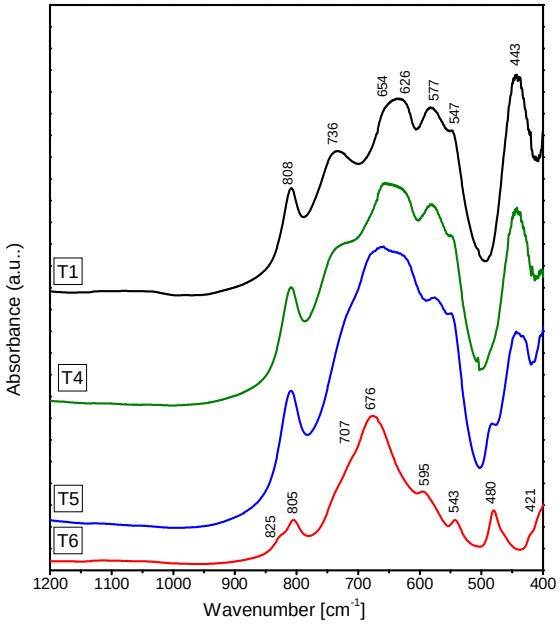

Figure 5.19. FT-IR spectra of $YTa_{1-x}Nb_xO_4$ samples prepared with different activator concentration

It can be noted that the FT-IR spectra contain no specific vibration modes corresponding to the SO_4 structural unit i.e. the stretching (1140-1080 cm^{-1}) and the bending (680-610 cm^{-1}) vibrations; sulphate intermediates were totally removed during the washing stage. FT-IR spectroscopy completes the structural information obtained from the XRD investigations.

5.2.2. Flux nature and thermal treatment influence

Structural characteristics

The synthesis parameters and the structural, morphological and luminescent characteristics for the $YTaO_4$:Nb samples are presented in table 5.4. XRD patterns and FTIR spectra of the $YTaO_4$:Nb powder samples prepared at 1200°C-1400°C with Li_2SO_4 and /or Na_2SO_4, as a flux are presented in figures 5.21-5.24

The most homogeneous $YTaO_4$:Nb powder was obtained at 1200^0C, using Li_2SO_4 as a flux. Sample T7, $YTaO_4$:Nb [Li_2SO_4; 1200°C] is a single phase material, consisting of monoclinic M prime polymorph, as seen from figure 5.21. At the same temperature, but replacing Li_2SO_4 with Na_2SO_4 as a flux, (sample T9) additional reflections can be observed. These reflections can be ascribed to the T' crystalline phase and show that, at 1200ºC, Na_2SO_4 does not ensure the complete polymorphous transformation of the tetragonal T' structure into the monoclinic M' structure of $YTaO_4$:Nb.

Table 5.4. The synthesis parameters and the structural, morphological and luminescent characteristics of the $YTaO_4$:Nb samples

Sample	Synthesis conditions		Characteristics			
	Flux	Firing regime	Crystalline structure	$D_{crystallites}$ (nm)	$D_{particules}$ - L/l (μm)	Emission I_{390} (%)
T7	Li_2SO_4	1200°C/4 h	M’	30	2-4 / 1-2	125
T8	Li_2SO_4:Na_2SO_4	1200°C/4 h	M’	28	1-3	83
T9	Na_2SO_4	1200°C/4 h	M’+T’	27	0.2-1	61
T11	Li_2SO_4	1300°C/4 h	M’+M	37	4-5 / 2-3	116
T12	Li_2SO_4:Na_2SO_4	1300°C/4 h	M’+M	33	2-3	102
T13	Na_2SO_4	1300°C/4 h	M’+M	35	0.5-1	70
T15	Li_2SO_4	1400°C/4 h	M+T	41	10-15	77
T16	Li_2SO_4:Na_2SO_4	1400°C/4 h	M	40	2-4	75
T17	Na_2SO_4	1400°C/4 h	M	25	2-3	67

The infrared spectra, figure 5.23, confirm that the synthesis conditions i.e. the flux nature and the thermal treatment influence the crystalline order degree of the phosphors, as already illustrated by the XRD patterns.FT-IR spectra, registered in the 1000-400 cm^{-1} range, show a complex pattern, which could be evaluated according to a structure with more or less distorted TaO_6 units, which share edges with one another in the monoclinic modification of $YTaO_4$. The FTIR spectra sustain the XRD data for the samples prepared with different fluxes.

Sample T7 prepared with Li_2SO_4 possesses a single phase M’- structure, as illustrated by the well formed 439 and 808 cm^{-1} absorption bands, that are not characteristic to the M-phase –figure 5.23. In sample T9, obtained using Na_2SO_4 as a flux, the M’ phase still exists, but the crystalline structure is more disordered, as suggested by the FTIR spectra.

For the samples prepared using Li_2SO_4 as flux, by increasing the calcination temperature, the crystalline host lattice becomes more disordered. The XRD patterns illustrate that the T11 sample, $YTaO_4$:Nb [Li_2SO_4; 1300°C], is a mixture of M’ and M phases, whereas the T15 sample, $YTaO_4$:Nb [Li_2SO_4; 1400°C], is predominantly a mixture of M and T phase – figure 5.24. The FT-IR analysis confirm the polymorphic transformation. The increase of the calcination temperature induces the conversion of M’ into M phase, process that is shown by the disappearance of the 439 cm^{-1} band and the diminishing of the 808 cm^{-1} band – figure 5.25.

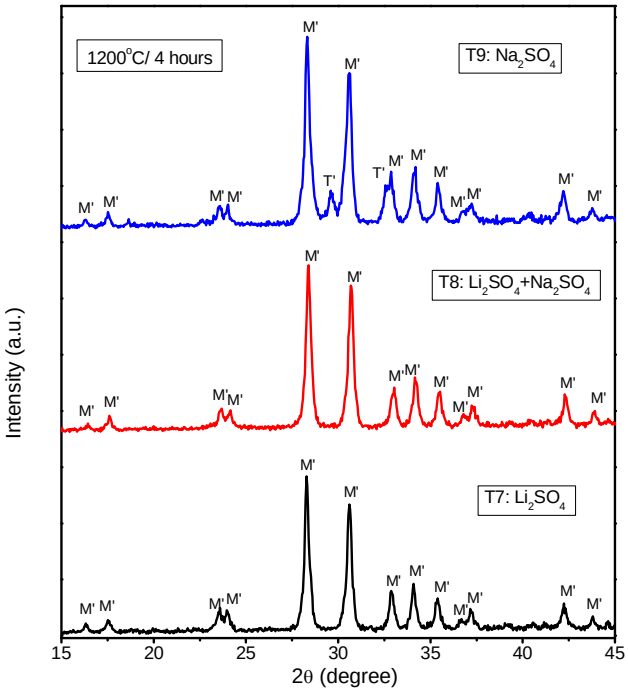

Figure 5.22. X-ray analysis of samples prepared with different flux nature, 1200°C/ 4 hours

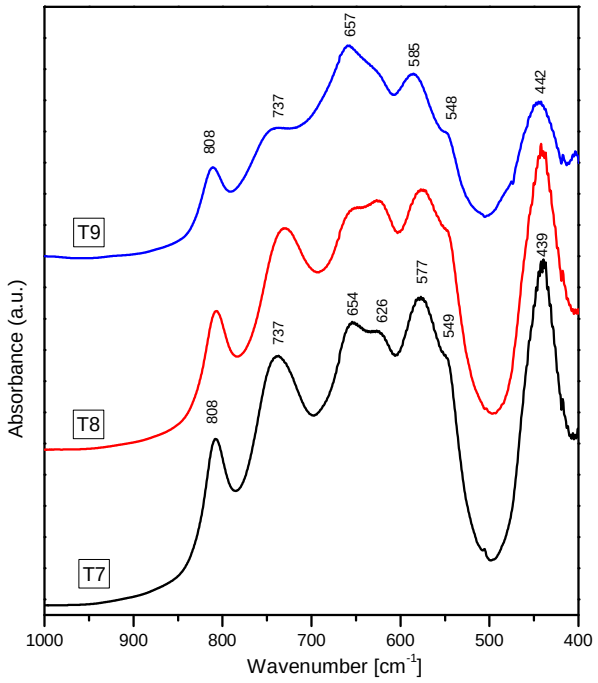

Figure 5.23. FT-IR spectra of samples prepared with different flux nature, 1200°C/ 4 hours

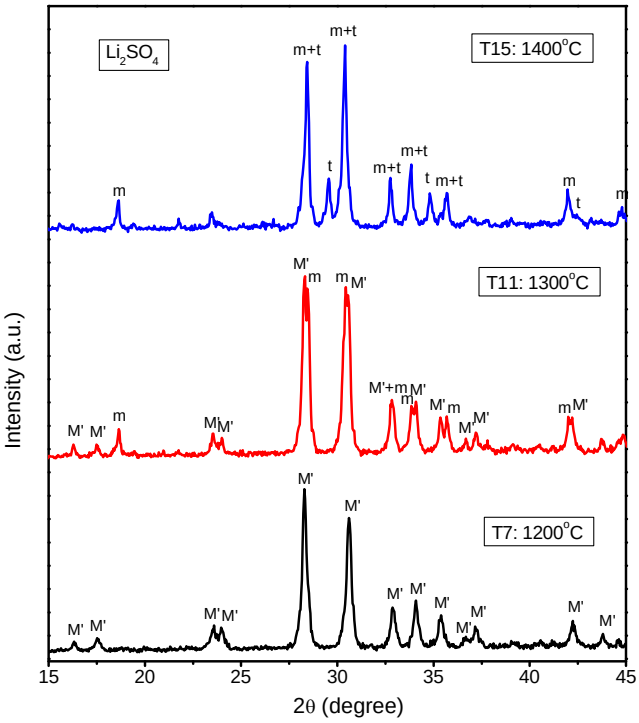

Figure 5.24. X-ray diffractograms corresponding to samples prepared at different calcination temperatures:1200°, 1300°, 1400°, using Li_2SO_4 as flux

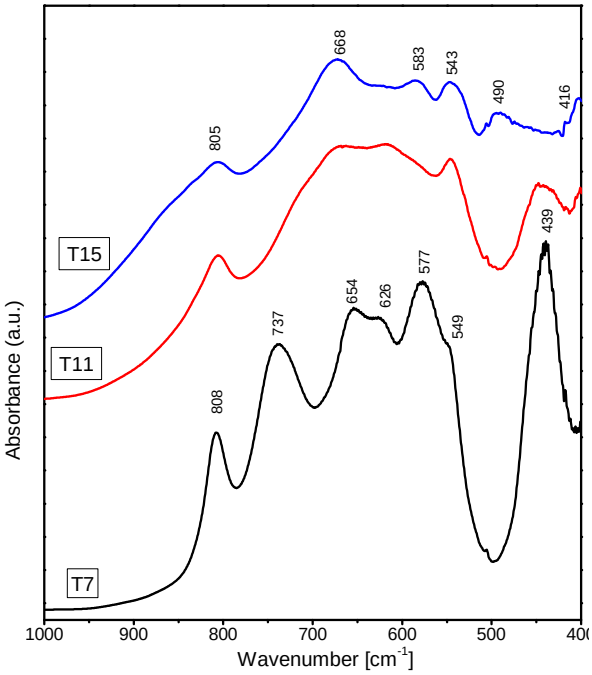

Figure 5.25. FT-IR spectra of the samples prepared at different calcination temperatures: 1200°, 1300°, 1400°, using Li_2SO_4 as flux

Morphological characteristics

The PL intensity is strongly affected by the crystalline homogeneity and phosphor powder particle size. A series of *SEM images* (figure 5.26) was made to characterize and compare the particle morphology and sizes for $YTaO_4$:Nb samples prepared under different synthesis conditions.

Samples prepared with Li_2SO_4 as a flux, under different thermal treatment regime (T7, T11 and T15), present variable morphology and particle sizes. By increasing the calcinations temperature (T15 sample), the particles shape becomes nearly spherical and they trend to aggregate as clusters. The particle size increases and most of them are of about 10-20 μm.

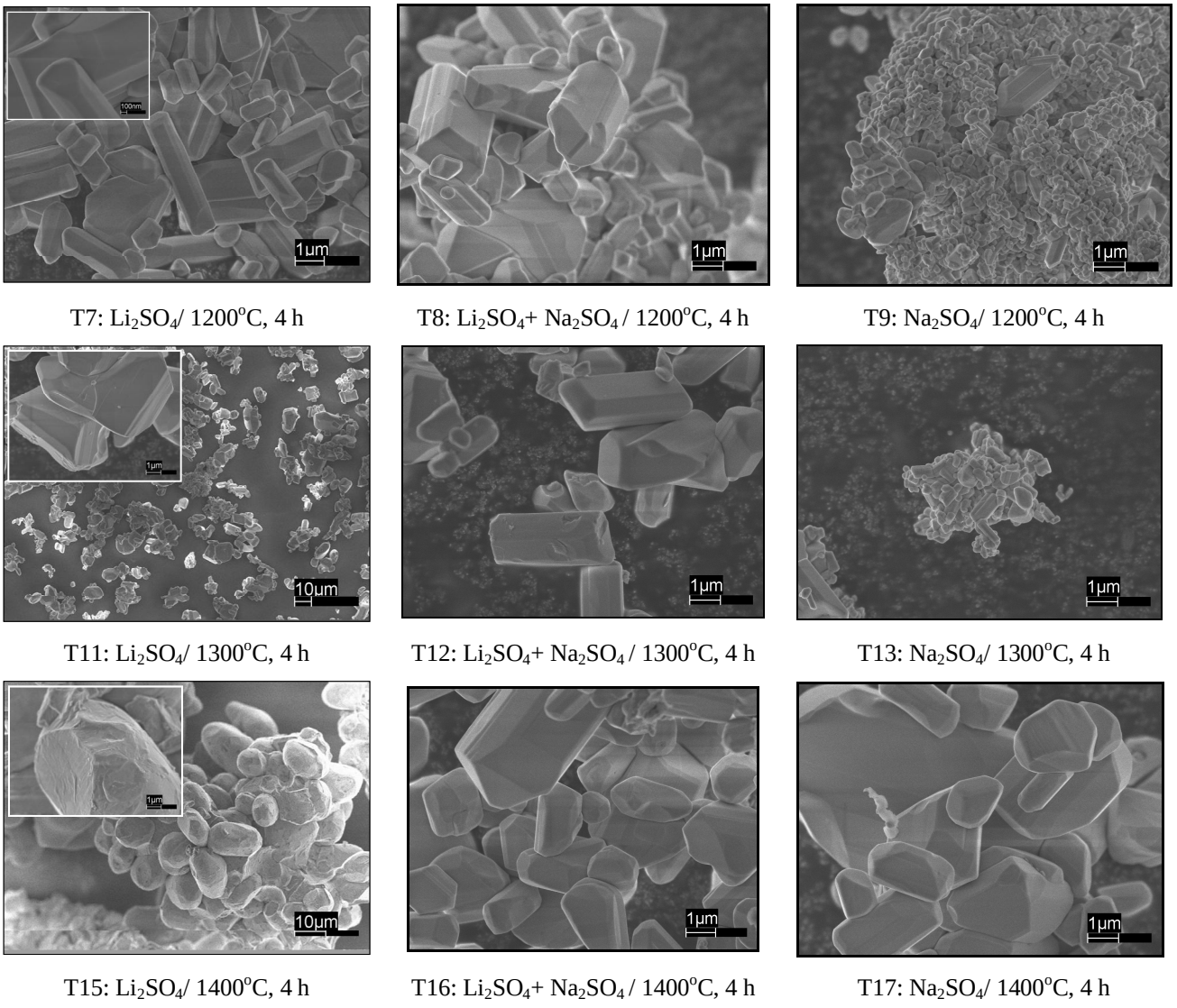

T7: Li_2SO_4/ 1200°C, 4 h | T8: Li_2SO_4+ Na_2SO_4 / 1200°C, 4 h | T9: Na_2SO_4/ 1200°C, 4 h

T11: Li_2SO_4/ 1300°C, 4 h | T12: Li_2SO_4+ Na_2SO_4 / 1300°C, 4 h | T13: Na_2SO_4/ 1300°C, 4 h

T15: Li_2SO_4/ 1400°C, 4 h | T16: Li_2SO_4+ Na_2SO_4 / 1400°C, 4 h | T17: Na_2SO_4/ 1400°C, 4 h

Figure 5.26. SEM images of $YTaO_4$:Nb samples

The scanning electron microscopy evidences the physical differences between M' and the other crystalline phases formed during the thermal treatment of the niobium tantalate phosphors. Generally, the M' phase crystals grow in regular, non-agglomerated polyhedral particles.

Luminescent properties

The luminescence colour and intensity of $YTaO_4$:Nb strongly depend on the niobium concentration, flux nature and calcination temperature (Table 5.4). All the powder samples are white in colour and almost all present blue luminescence under 254 nm excitation. The observed luminescence has a short decay time which does not last after the excitation stops. The partial or total replacement of tantalum with niobium atoms strongly improves the sensitivity to UV radiation resulting in a substantial intensification of the photoluminescence emission (samples T2-T6). Yttrium niobate (sample T6) shows the strongest emission (λ_{max}=395 nm) behaving as a good self-activated phosphor. From niobium activated yttrium tantalate series samples, the one prepared with 15 mole % niobium shows the highest emission intensity and is considered as an internal standard for the rest of the samples.

Typical emission spectra are presented in Figure 5.27, for $YTaO_4$: Nb samples prepared at different temperatures, with Li_2SO_4 as flux. In the insert image, the emission and excitation spectra of sample T7 are depicted. The excitation spectrum consists in a band with a maximum at around 260 nm, whereas the emission peak is situated at around 390 nm. One notes that the increase of the calcination temperature determines the decrease of the $YTaO_4$: Nb phosphor emission intensity.

The influence of the flux nature and firing regime on the photoluminescence (PL) relative intensity of the $YTaO_4$: Nb phosphor sample is presented in figure 5.28. The sample prepared at 1200^0C using Li_2SO_4 as a flux presents the highest luminescent intensity. When Li_2SO_4 - Na_2SO_4 mixtures or Na_2SO_4 are used as a flux, a relatively higher temperature (~1300^0C) is needed to obtain good luminescent properties. The different luminescence properties of the synthesized $YTaO_4$: Nb samples can be correlated with their crystalline structure and particle morphology and sizes.

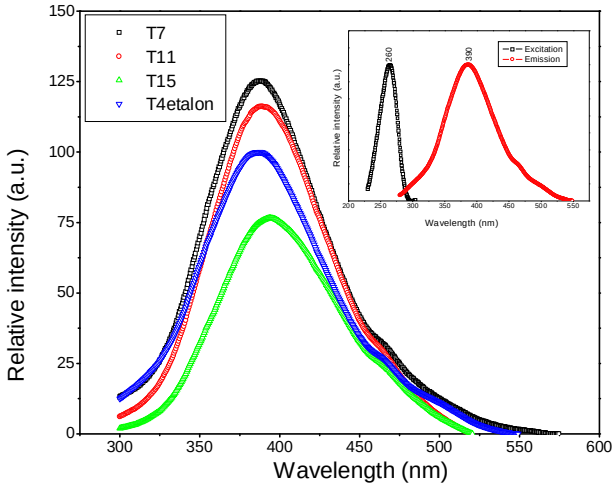

Figure 5.27. Emission spectra (λ_{exc} = 254 nm) for $YTaO_4$:Nb samples prepared with cu Li_2SO_4 as flux (sample T4 – internal standard)

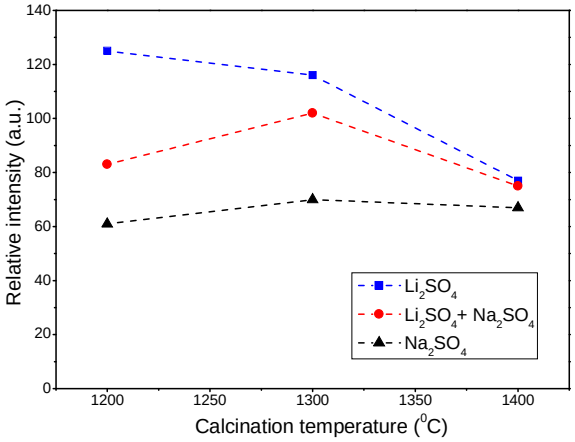

Figure 5.28. Flux nature and calcinations temperature influence on maximum of emission intensity for $YTaO_4$:Nb samples

By comparing the XRD data with the luminescence properties, one can observe that the sample prepared at 1200^0C using Li_2SO_4 as a flux, presents the highest luminescent intensity which can be associated with the M'-$YTaO_4$ phase. For the Y_2O_3-Ta_2O_5-Nb_2O_5 system, Na_2SO_4 shows weaker flux reactivity as compared with Li_2SO_4. This behavior is responsible for the weakest luminescence emission observed in this sample series. Moreover, the heterogeneity of the crystalline phases of T11 and T15 samples, could explain the decrease of the emission intensity with the increase of the calcination temperature. By heating, the M' phase could convert into T phase which, during the cooling stage, could transform into the M phase. The emission intensity of the samples prepared at higher temperatures is lower due to the beginning of the M' phase conversion.

5.3. Niobium and rare earth activated yttrium tantalate, $YTaO_4$:Nb/RE

The synthesis of $YTaO_4$:Nb/RE luminescent materials was achieved by solid state reaction route, as well.

5.3.3. Luminescent properties

The excitation and emission spectra of the samples have put into evidence the energy transfer that involves the host lattice – tantalate and niobate groups and the activator ions: Eu^{3+} and Tb^{3+}. Depending on the activator concentration (Eu^{3+} or Tb^{3+} ions) and their incorporation degree in the host lattice, the materials present emissions in different spectral domains.

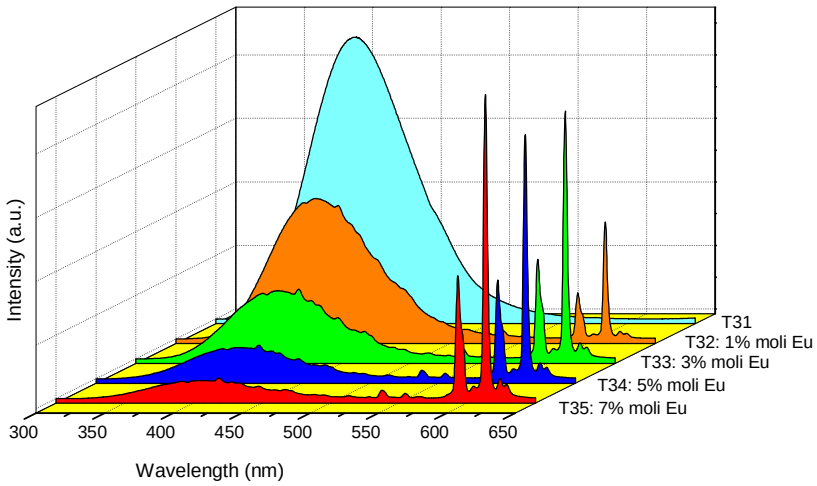

Figure 5.36. Emission spectra of $Y_{1-x}Eu_xTa_{0,85}Nb_{0,15}O_4$ samples

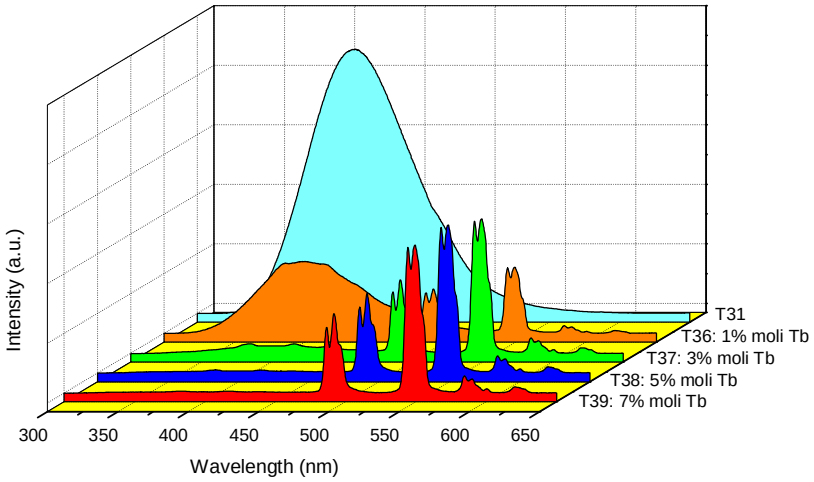

Figure 5.37. Emission spectra of the $Y_{1-x}Tb_xTa_{0,85}Nb_{0,15}O_4$ samples

The incorporation of the activator ions into the tantalate matrix brings about the specific luminescence, as illustrated by the emission spectra. The complexity of the spectra is correlated with the presence of bands corresponding to the electronic transitions: $^5D_0 \rightarrow {}^7F_1$ (~ 590 nm); $^5D_0 \rightarrow {}^7F_2$ (~ 615 nm) for Eu^{3+} and $^5D_4 \rightarrow {}^7F_6$ (~ 488 nm); $^5D_4 \rightarrow {}^7F_5$ (~ 545 nm); $^5D_4 \rightarrow {}^7F_4$ (~ 587 nm); $^5D_0 \rightarrow {}^7F_3$ (~ 621 nm) for Tb^{3+}.

CHAPTER 6: NIOBIUM ACTIVATED YTTRIUM TANTALATE THIN FILMS

Over the last few years, significant research interest in the growth and characterization of luminescent thin films has been conducted. Compared to powders, luminescent thin films offer several advantages due to their good luminescence characteristics, higher image resolution due to the

smaller grains, better thermal stability and good adhesion to the substrate. The research carried out for the synthesis and the characterization of the niobium activated yttrium tantalate, $YTaO_4$:Nb thin films presents a fundamental character, since-until now-the scientific literature does not present any information regarding this topic. Among the techniques used to deposit luminescent thin films, the Pulsed Laser Deposition (PLD) is a unique method for the stoichiometric ablation of the target material on a substrate, offering an excellent control of the film morphology.

6.1. Laser ablated $YTaO_4$ thin films

The experiments were supported by the European Community through a Marie Curie Individual Fellowship - ´ngstrom Laboratory, Materials Science Department, Uppsala University, Sweden.

6.1.1. Experimental set-up

Thin films were grown by the PLD technique using an ArF excimer laser Lambda Physic LPX 200 with a wavelength of 193 nm. The experimental set-up consists in a stainless steel cylindrical cross-shaped deposition chamber, equipped with an additional window for the laser beam, as shown in figure 6.1. The laser beam was focused onto the target by a quartz lens (focal length = 13 cm). The laser energy density was 1.5 J/cm^2 and the repetition rate was varied between 1 to 20 Hz.

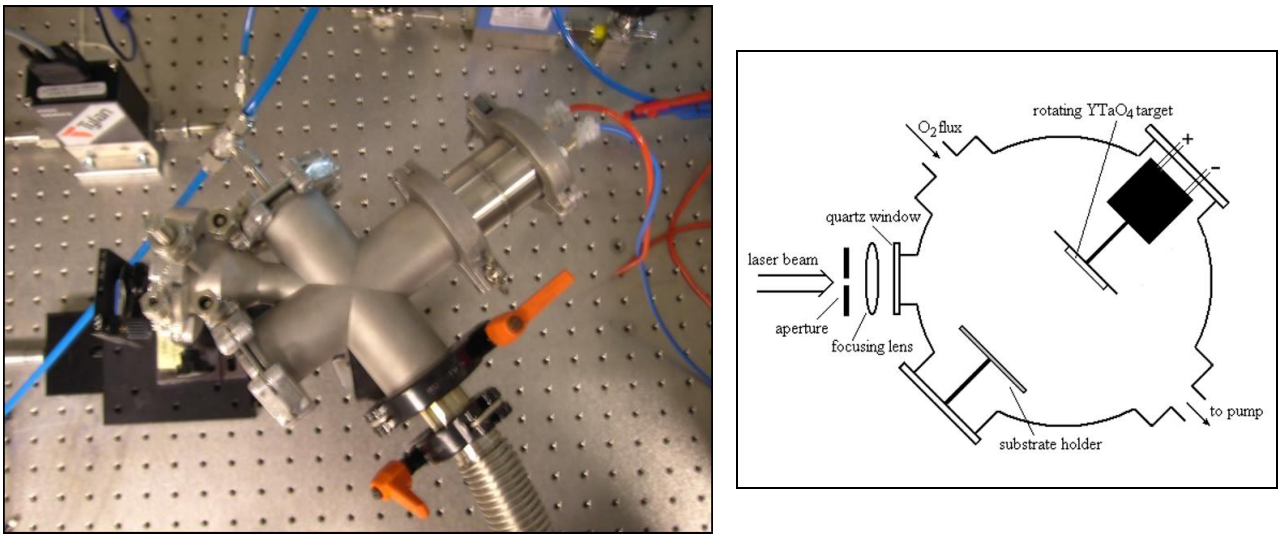

Figure 6.2. Photografic image (left) and cross-section view (right) of the ablation experimental set-up

Niobium activated yttrium tantalate targets were prepared from monoclinic $YTaO_4$:Nb (15 mole % niobium) powder. The powder mixture was compacted into pellets (Ø = 12 mm, thickness = 2 mm) and sintered at 1200^{0}C for 8h to obtain dense, crystalline M'-$YTaO_4$:Nb ablation targets. During the deposition process the laser beam hits the target at an incidence angle of 45^0. The substrate and the target were parallel and opposite to each other in the deposition chamber. The target

was rotated during the ablation process. The distance between the target and the substrate was kept at 30 mm. The normal pressure in the vacuum chamber during the film deposition was 0.5 mTorr with a perpendicular oxygen flow of 1.04 ml/min to the target-substrate direction. All the depositions were performed at room temperature. A post-deposition annealing treatment of the $YTaO_4$:Nb films was performed at 900^0C for 1-4 hours.

6.1.3. $YTaO_4$:Nb thin films characterization

Structural characteristics of the thin films were determined by X-ray Diffraction (XRD) and electron diffraction patterns obtained in a transmission electron microscope (TEM). The X-ray Diffraction was performed with a parallel beam set-up using a $Cu_{K\alpha}$ radiation, in the range of $2\theta = 10 - 90^0$. TEM analysis (200 kV accelerating voltage) was also used to obtain crystallite size and crystallinity of single particles.

Scanning Electron Microscopy, SEM analysis was performed using a LEO 1550 microscope, equipped with an in-lens detector and a field-emission gun.

The luminescent properties of the yttrium tantalate ablation target and thin films were evaluated on the basis of the emission spectra, using a Perkin-Elmer, LS 45 spectrophotometer.

6.1.3.1. Structural characterization

Figure 6.6-7 presents the diffractograms of the ablation target, the as-deposited thin films (1.5 J/cm^2 fluency, 10 Hz frequency) and annealed thin films (900^0C / 2 hrs). The ablation target has a monoclinic M'-$YTaO_4$:Nb crystalline structure. The diffractograms of the as-deposited thin film showed a semi-crystalline material, with weak diffraction lines corresponding to the monoclinic M' structure of $YTaO_4$:Nb and to the Y_2O_3 structure(*).

The presence of the Y_2O_3 crystalline phase is associated with the presence of an amorphous Ta_2O_5 phase in the as-deposited thin film. The annealing process ensures the complete transformation of the Y_2O_3 crystalline and Ta_2O_5 amorphous phases, into a single crystalline phase M'-$YTaO_4$:Nb. By comparison with the as-deposited thin film, the annealed thin film presents a structure with a higher crystalline order. In spite of the fact that the niobium activated yttrium tantalate target presents some structural peculiarities (two monoclinic phases M and M', respectively and one tetragonal phase T), the monoclinic M'-$YTaO_4$:Nb crystalline structure is preserved during the PLD process.

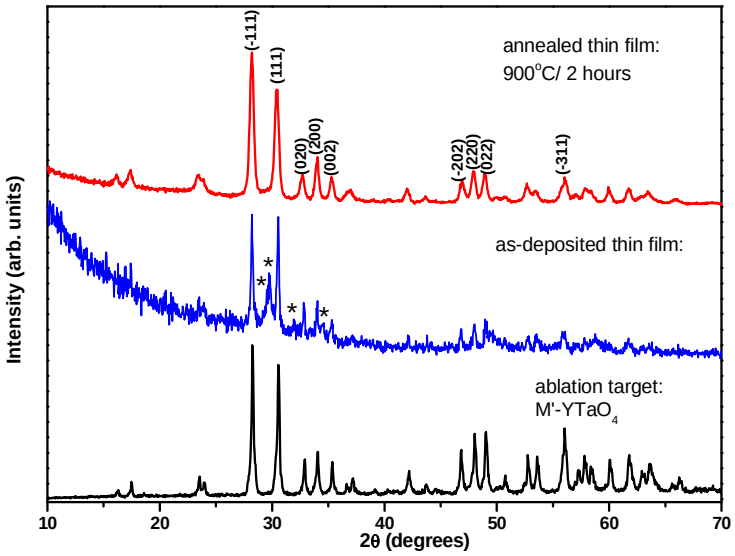

Figure 6.6-7. X-ray diffractograms of ablation target, as-deposited thin film and annealed thin film

The *TEM images* with the corresponding electron diffraction pattern (insert) of the niobium activated yttrium tantalate thin films are presented in figure 6.12. The bright field micrographs of the as-deposited thin film revealed a small crystallite size, while the corresponding electron diffraction pattern shows an amorphous structure, figure 6.12 a.

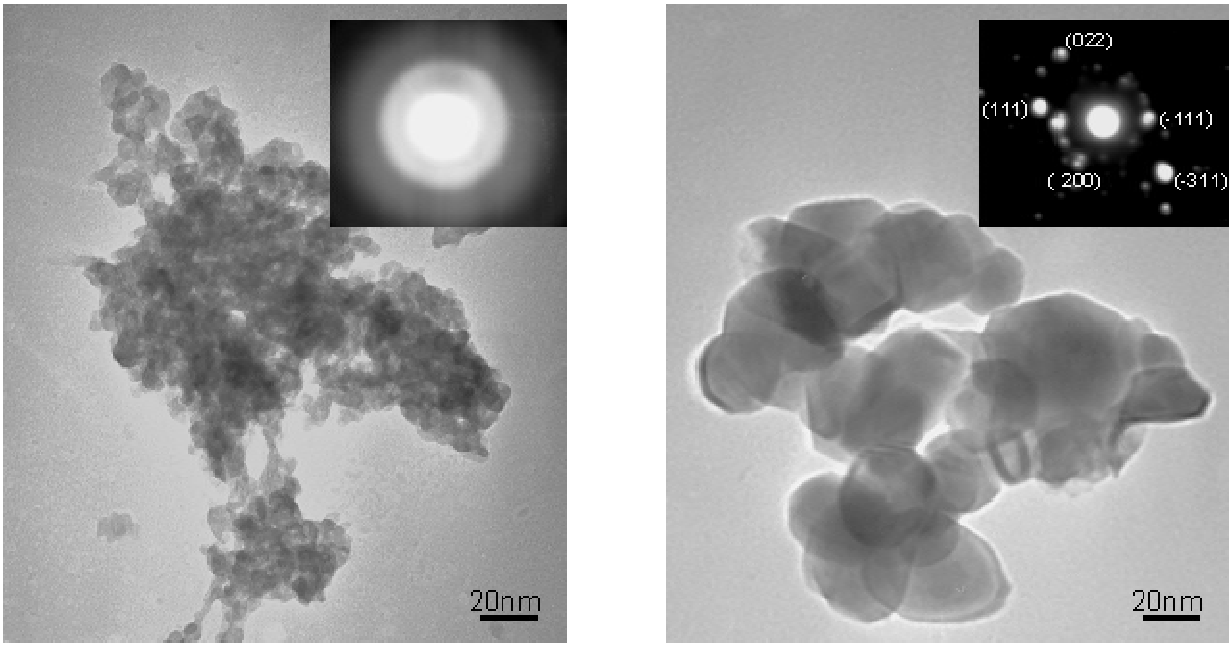

a B

Figure 6.12. TEM micrographs and electron diffraction pattern (inset) of:
as – deposited (a) and annealed (b) $YTaO_4$:Nb thin films

As the TEM micrograph of the annealed film shows nearly spherical grains of about 20-40 nm diameters, being the building blocks that form the thin film - figure 6.12 b.

The electron diffraction pattern of this thin film presents distinguishable diffraction spots. It is clear that the particles are single crystalline, but the instrumental limitations makes probable that the diffraction patterns obtained from TEM - figure 6.12 b originates from more than one single crystalline particle, but most probably two, or-at most-three particles. XRD and TEM analysis show that the annealing process induces an improvement of the crystalline order of the thin film structure.

6.1.3.2. Morphological characteristics

A series of *SEM images* - figures 6.13 and 6.15 - was performed to characterize and compare the particle morphology and sizes for the as-deposited and annealed $YTaO_4$:Nb thin films, respectively.

The as-deposited film presents a porous morphology and a high degree of agglomeration of the deposited particles. The particles do not have so well defined morphology and one can observe the similarity in size - figure 6.13. For the annealed film a sintering effect can be observed. Well-defined grains are formed and their shape becomes more spherical and uniform The grain sizes are of about 20-40 nm in diameter, figure 6.16.

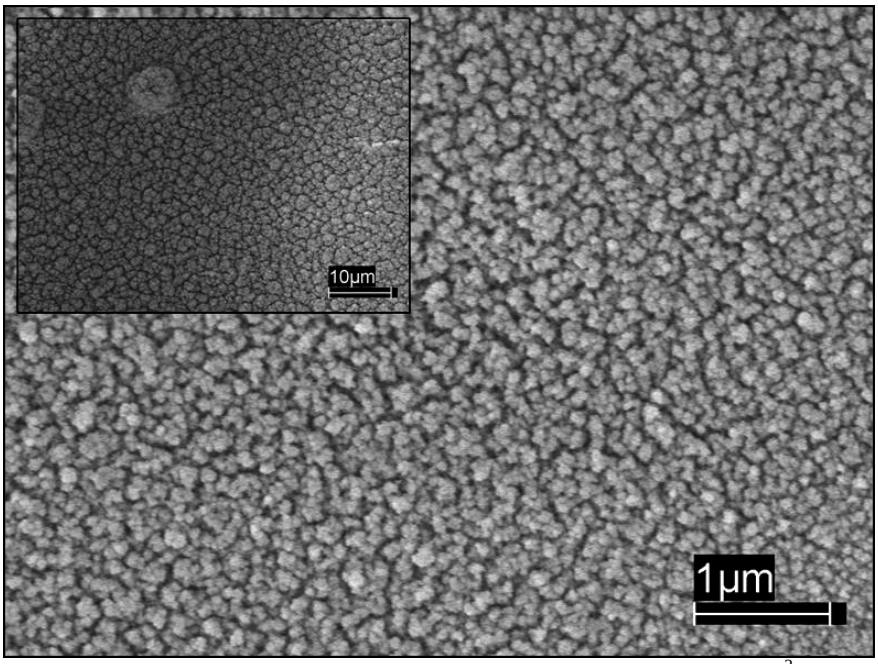

Figure 6.13. SEM images of deposited thin film: 30 minutes (Φ = 1,533 J/cm^2, f = 10 Hz)

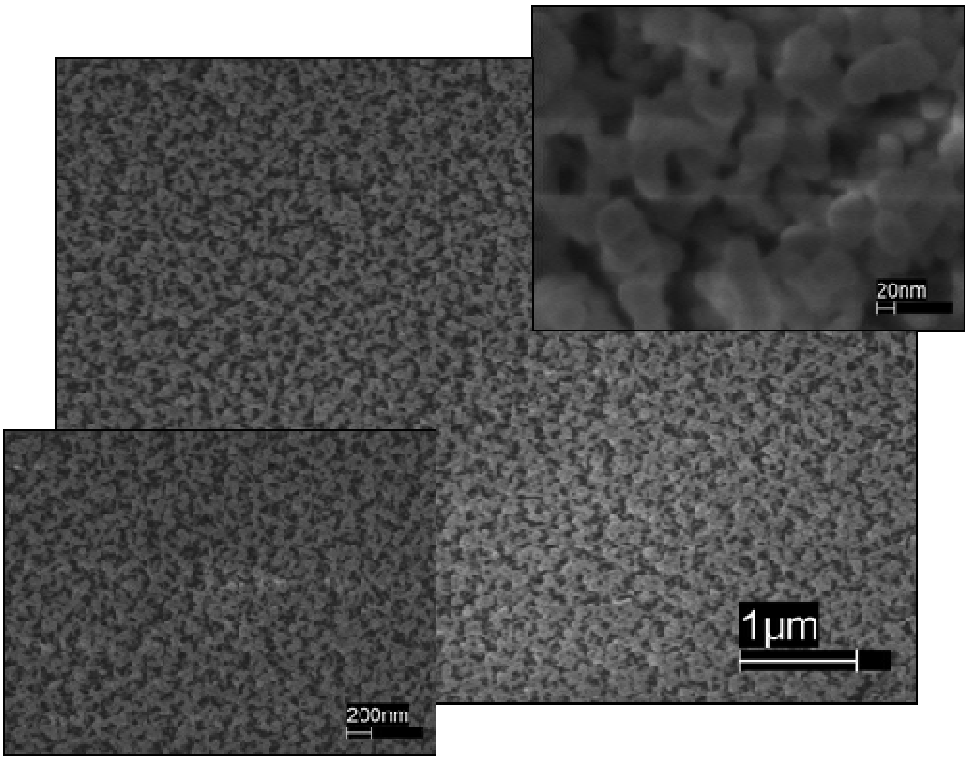

Figure 6.16. SEM images of the annealed thin film 900°C/2 hours

The luminescence properties of $YTaO_4$:Nb originates from the different luminescent centers of the tantalate and niobate groups. Figure 6.19 presents the emission spectra of the $YTaO_4$:Nb ablation target and $YTaO_4$:Nb annealed thin films under short UV excitation (λ = 229 nm).

The ablation target shows a maximum in emission at around 400 nm which is in agreement with the luminescent characteristics of the M'-$YTaO_4$:Nb powders. It must be mentioned that the as-deposited $YTaO_4$:Nb thin film does not present a noticeable luminescence emission. The luminescence spectrum collected from the annealed films shows a maximum of emission intensity at 385 nm maintaining the characteristic domain of the $YTaO_4$:Nb powders. One can observe that the maximum of the emission intensity is shifted about 15 nm. This shift is related to the nano-sized nature of the thin film. These nano-crystalline characteristics of the particles change the ratio between the different luminescent centres in the tantalate and niobate groups.

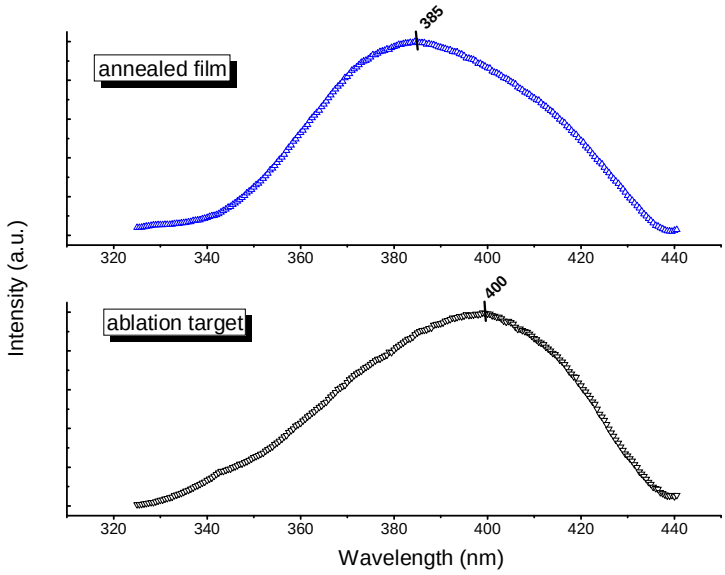

Figure 6.19. Emission spectra ($\lambda_{exc.}$ = 229 nm) of the ablation target and annealed thin film, (Φ = 1,533 J/cm^2, f = 10 Hz, 900^{o}C/ 2 hours)

The annealing treatment applied on the as-deposited thin film strongly improves its luminescent characteristics and is directly correlated with the formation of the monoclinic M' structure.

6.1. Chemical Solution Deposition of the $YTaO_4$:Nb Thin Films

Lately, the chemical solution deposition of rare earths tantalate and niobate thin films using alkoxide-type precursors has gained scientific interest. Recent studies have revealed the importance of these oxide thin films for the fabrication of superconducting multilayer architectures [10].

These experiments have been performed within the Materials Science Laboratory, Technical University of Cluj-Napoca and represent preliminary experiments, the fabrication of $YTaO_4$:Nb thin films with adequate properties for optical applications obtained by chemical methods requiring supplementary studies.

6.2.1. Preliminary studies on the coating solution preparation

Within this approach, the choice of the reagents for the synthesis of the precursor solution has required an accurate analysis of the chemical reactivity of Y^{3+} and Ta^{5+} cation supplying salts. Under these circumstances, taking into consideration the complex polymorphism of yttrium tantalate, as well, the previously $YTaO_4$:Nb prepared, calcined and characterized powders (Chapter 5) have been used. The choice of the TFA-MOD method has been considered taking into account the strength of the trifluoroacetic acid, CF_3-COOH, one of the strongest organic acids [13].

6.2.2. Characterization of the precursor solution

Analogue to the literature data for other oxide compounds, it can be assumed that the obtained precursor solution is a mixture of yttrium, tantalum and niobium trifluoroacetates[12].

The chemical reaction involved in the formation of the precursor solution is:

$$YTa_{0,85}Nb_{0,15}O_4+8CF_3\text{-}COOH \rightarrow Y(CF_3\text{-}COO)_3 + 0,85Ta(CF_3\text{-}COO)_5 + 0,15Nb(CF_3\text{-}COO)_5 + 4H_2O$$

The FT-IR spectrum of the precursor solution is presented in figure 6.23. The assignments have been made using the literature data. The large band between 3750 and 3250 cm^{-1} is attributed to the stretching vibrations of the O-H bonds. The C-F bonds due to the yttrium, tantalum or niobium trifluoroacetates are found at 1230, 1166, 815 and 784 cm^{-1}, respectively. The displacement of the vibrations corresponding to the C-F bond towards higher frequencies indicates the ligand character of the trifluoroacetic acid. The precursor powder exhibits the characteristic vibrations for the carboxilate (COO^-) ion at 1628 and 1537 cm^{-1}, respectively. The peaks beneath 815 cm^{-1} are attributed to the stretching vibrations corresponding to the Me-O bonds.

The literature data describe the decomposition of the metal trifluoroacetates in the temperature range 150-450^oC [13]. Thus, under dry atmosphere, the trifluoroacetates decompose directly into fluorides, according to the general reaction equation given below:

$$M(CF_3COO)_x \rightarrow MF_x,$$

where: M – metal, x - metal valence

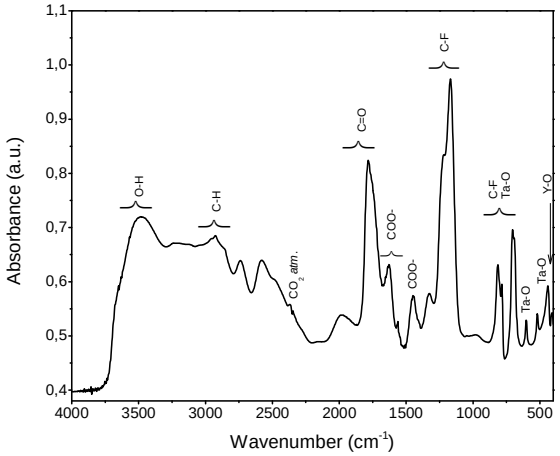

Figure 6.23. FT-IR Spectrum of the precursor solution

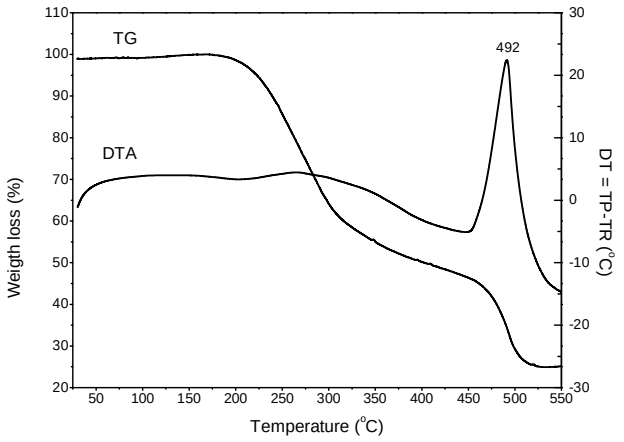

Figure 6.24. TG-DTA Curves corresponding to the precursor solution

In humid atmosphere, the decomposition of the trifluoroacetates is more complex, the formation, in a first step, of metal oxyfluorides being registered in agreement with the general transformation sequence given below:

$$M(CF_3\text{-}COO)_x \rightarrow M\text{-}O\text{-}F \text{ (amorphous)} + C\text{-}O\text{-}F \text{ (volatile rezidues)}$$

Further, with the increase of temperature, due to the humid atmosphere as well, the oxyfluorides decompose to the corresponding oxides with the formation of hydrofluoric acid [13].

The TG analysis of the dried coating solution– figure 6.24- demonstrates that the decomposition of trifluoroacetates takes place in two steps. In the temperature range 150-450^{o}C a substantially weight loss of 52,92% which can be attributed to the combustion of the organic parts takes place, in agreement with the reactions given below:

$Y(CF_3\text{-}COO)_3 \rightarrow Y\text{-}O\text{-}F$ (amorphous) + C-O-F (volatile residue)

$Ta(CF_3\text{-}COO)_5 \rightarrow Ta\text{-}O\text{-}F$ (amorphous) + C-O-F (volatile residue)

$Nb(CF_3\text{-}COO)_5 \rightarrow Nb\text{-}O\text{-}F$ (amorphous) + C-O-F (volatile residue)

Further on, in the temperature range 450-525^{o}C the exothermic peak observed on the DTA plot indicates a complex process of chemical interaction between the oxyfluorides with the formation of the yttrium tantalate crystalline lattice, associated with the evolvement of fluorine as hydrofluoric acid.

6.2.2. The deposition and characterization of $YTaO_4$:Nb thin films

The deposition of the thin films has been performed by spin-coating on two types of single crystalline substrates: Si(111) and $SrTiO_3$ (STO). A single step post-deposition pyrolysis and crystallization thermal treatment has been performed to obtain the luminescent thin film.

The X-ray diffraction patterns of the films deposited on Si(111) and (100) STO substrates are presented in figures 6.28 and 6.29. It is to be noticed the relative weak crystallinity of both films, the presence of several corresponding reflections attributed to $YTaO_4$ stating for the beginning of the crystallization process. Thus, in the diffractograms of the film deposited on Si, except for the reflections due to the substrate, the reflections correspond to the (-111) and (111) planes-for the monoclinic structure M' of yttrium tantalate, (210) and (211) – for the tetragonal structure T.

The indexation has been made using the JCPDS database, PDF nr. 24-1425 for M'-$YTaO_4$, and JCPDS PDF nr. 26-1478 for T-$YTaO_4$, respectively. The reflections corresponding to the two structures M' and T of $YTaO_4$, but with a diminished intensity are found in the diffractogram of the

film deposited on the STO substrate, as well. Taking into consideration the polymorphism observed at the synthesis of $YTaO_4$, the tetragonal structure formation can be correlated with the thermal treatment parameters: maximum temperature and calcination time.

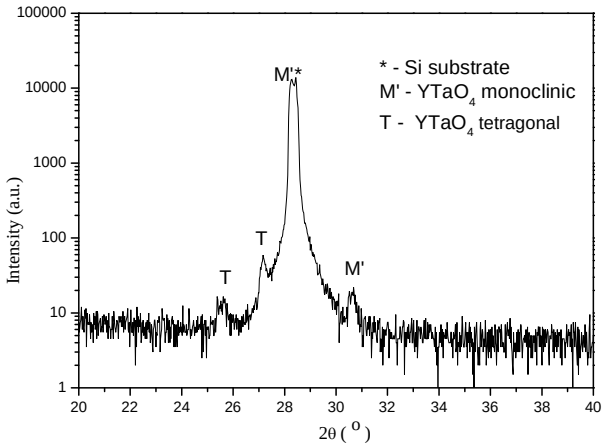

Figure 6.28. X-ray diffraction pattern of the film deposited on Si substrate

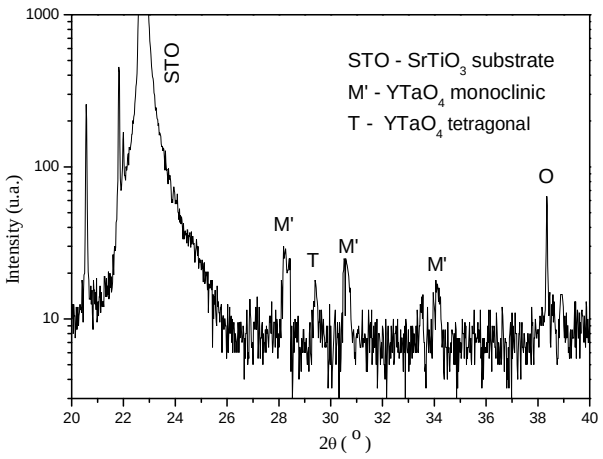

Figure 6.29. X-ray diffraction pattern of the film deposited on STO substrate

The atomic force microscopy investigations of the obtained films are presented in figures 6.30, 6.31. The differences between the two substrates, regarding both the chemical nature and the physical-structural properties determine a completely different surface morphology, as evidenced by atomic force microscopy.

The thin film deposited on silicon is continuous, with a roughness of about 0.22nm. For comparison, the thin film deposited on STO is not continuous, island formation being observed, the surface roughness is about 25 nm. These morphological characteristics can be correlated with the different degree of the two surfaces. The defects observed for the thin film deposited on STO can be attributed to the substrate, which, prior to the deposition, was chemically treated.

The different structural and morphological characteristics of the two thin films are reflected in their emission spectra -figures 6.32. a and b.

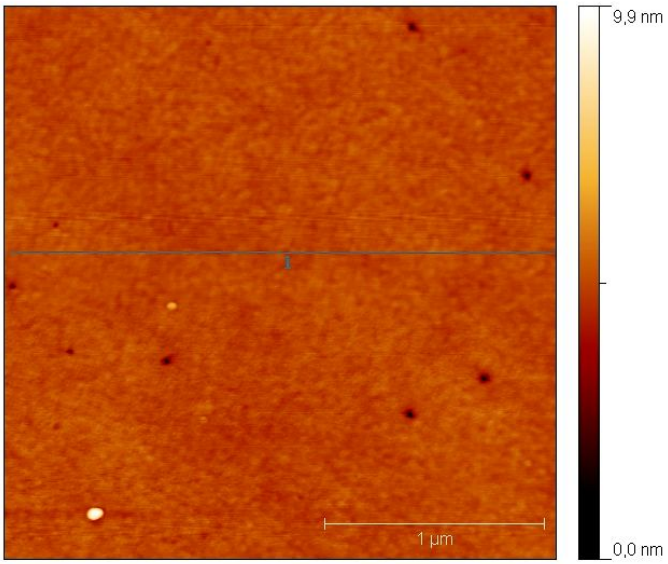

A

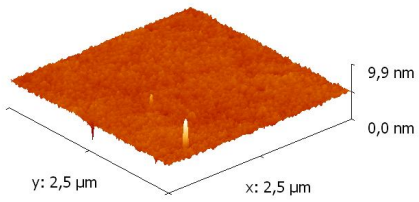

b

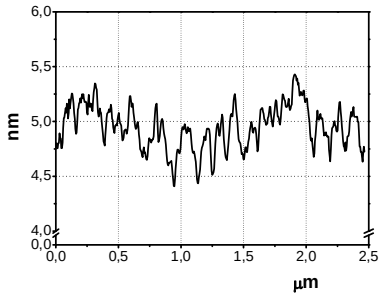

c

Figure 6.30. AFM images for the thin film deposited on Si substrate: 2D (a), 3D (b) and surface morphology profile (c)

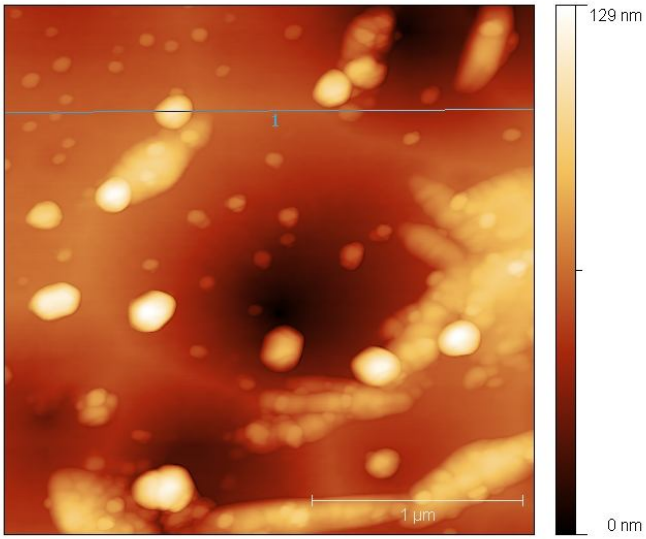

A

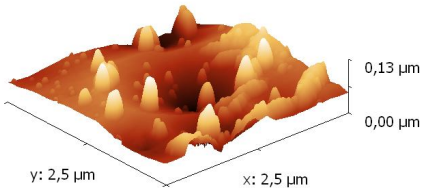

b

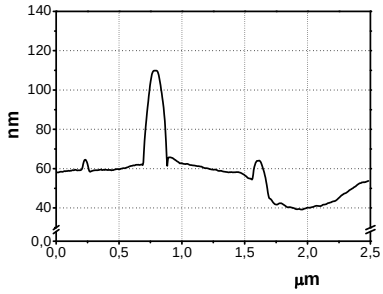

c

Figure 6.31. AFM images for the thin film deposited on STO substrate: 2D (a), 3D (b) and surface morphology profile (c)

The thin film deposited on Si(111) presents an emission maximum at a wavelength of 400 nm, and the spectrum shape is similar with that of the thin films deposited by laser ablation.

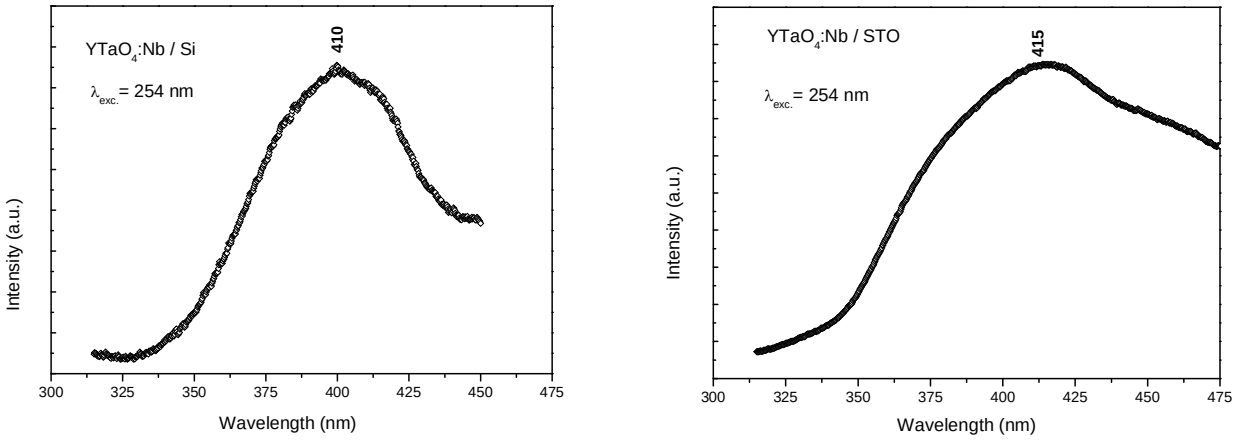

Figure 6.32. Emission spectra of the deposited thin films

Comparatively, the shape of the spectrum registered for the thin films deposited on STO is different, and the emission maximum is shifted towards higher wavelength around 415 nm.

CONCLUSIONS

The thesis presents the original results on the preparation of $YTaO_4$ -based host powders and thin films with luminescent properties. The powder oxide material was synthetized by solid state reaction, structurally, morphologically, optically characterized and further used for the deposition of luminescent thin films. The oxide thin films were deposited on single crystalline Si and $SrTiO_3$ substrates by laser ablation and chemical solution deposition using trifluoroacetate-based precursors. The structural, morphological and optical-luminescent properties of the as-obtained thin films were investigated.

Conceptually, the thesis has an unitary character, the investigations being oriented towards the study of yttrium tantalate powders and thin films. The optimum synthesis/ deposition conditions for powder/thin films were established through a double correlation composition-structure-properties.

The studies performed on the oxide powders have enabled the identification of the influence of the preparation factors, such as: the mineralizing agent, calcination temperature, activator ions concentration on the structural, morphological and luminescent characteristics of the synthesized materials: *$YTaO_4$*, *$YTaO_4$:Nb* and *$YTaO_4$:Nb/RE*. In this respect the original researches comprise studies regarding:

- *The calcining temperature ($900^oC \div 1400^oC$) and time (2÷6 hours) influence*, to determine the optimum values corresponding to the two parameters necessary to obtain a high quality luminescent material. Thus, the complex polymorphism of yttrium tantalate has been analyzed: T'→ M'→T→M and the optimum thermal treatment leading to a single phase polycrystalline material has been established to be1200^oC / 4 hours.
- The *effect of the nature of the mineralizing agent*– alkaline metal salts: Li_2SO_4, Na_2SO_4 and a 1:1 Li_2SO_4 + Na_2SO_4 molar ratio mixture. The investigations have enabled the direct correlation of the structural and morphological characteristics with the luminescent characteristics of $YTaO_4$ and $YTaO_4$:Nb, respectively;
- *The nature and concentration of the activator(s) ion(s)*: Nb^{5+}, Nb^{5+}/Eu^{3+} and Nb^{5+}/Tb^{3+} reflected in the analysis of the incorporation degree of the activator in the host lattice, as well as the identification of the luminescence centers corresponding to the host lattice-activator(s) system.

The investigation techniques used were: X-ray diffraction, IR spectroscopy, optical microscopy, scanning electronic microscopy and luminescence spectroscopy. By comparing the structural, morphological and luminescent characteristics of the samples it has been observed that the fabrication of a material with superior optical material and, consequently, high application potential is associated with the formation of a monoclinic structure M' for the $YTaO_4$ host lattice.

The deposition, for the first time, both by physical-laser ablation and chemical solution deposition using trifluoroacetate type precursors of niobium activated yttrium tantalate thin films confers originality to this thesis.

The original contributions regarding thin films envisage:

- *Laser ablation (PVD):*
  - The establishment of experimental geometry and of the deposition conditions: energy density, laser frequency, pressure, oxygen flow in the ablation chamber. The grain size distribution of the ablated sample has enabled to establish the value of the laser energy density necessary for the ablation process.
  - The analysis of the mechanism of the ablation process regarding the laser-target interaction, plasma composition and growth mechanisms.

- The optimization of the post-deposition thermal treatment /temperature-time/necessary for the mobility enhancement of the deposited atoms for the reconstruction of the yttrium tantalate lattice.
- The correlation of the XRD and TEM structural and SEM, TEM morphological investigations evidencing the nanocrystalline nature of the thermally treated $YTaO_4$:Nb thin films.
- The investigation of the luminescent properties of the thermally treated thin films by luminescence spectroscopy.

- *Chemical solution deposition method:*
  - Trifluoroacetate-type precursor coating solution synthesis and characterization by means of FT-IR spectroscopy and TG-DTA thermal analysis;
  - Optimization of the thin films deposition conditions from the precursor solution: the choice of the viscosity enhancement agent and the spinning schedule;
  - Post-deposition single-step thermal treatment optimization for the film crystallization;
  - Comparison among the structural (XRD), morphological (AFM) analyses and luminescent properties (LP) of the thin films deposited on single crystalline Si (111) and $SrTiO_3$(100);

The formation of $YTaO_4$ after the post-deposition thermal treatment states for one characteristic of both methods, namely a good stoichiometric transfer of the cationic species from the target to the film.

The structural and morphological characteristics–nanometric dimensions of the particles, and crystallites as well, modify the ratio between the luminescence centers of the tantalate and niobate units, evidenced by the excitation and emission spectra of the films deposited both by physical and chemical methods.

Supplementary experiments are necessary to conclude on the correlation composition-structure-properties for the two deposition methods in order to improve the luminescent properties and to evaluate the applicative potential of the $YTaO_4$:Nb nano-crystalline thin films in the field of X-ray medical imagistics.

The simplicity, compositional versatility, scalability of the studied chemical solution deposition method leads to the enlargement of the applicative potential towards new directions, such as: luminescent multilayer architectures and their applications in the elaboration of new compounds in the Y_2O_3-Ta_2O_5 (Y_3TaO_7) system used as epitaxial buffer layer in high temperature superconducting coated conductors.

The results of the thesis have been published in four scientific papers and two others are in press. The four published papers, as well as the list of relevant papers of the author in the field of oxide materials synthesis are found in the annex.

SELECTED REFERENCES:

Chapter 3

1. G. Blasse, B. C. Grabmaier – Luminescent Materials, Springer-Verlag, Berlin- NewYork, 1994
2. S. L. Issler , C. C. Torardi, *J. Alloys Comp*. 229 (1995) 54-65
3. R.C. Ropp – Luminescence and the Solid State, Elsevier, Amsterdam–Oxford-New York–Tokyo, 1991
8. W. D. Callister, Jr. – Materials Science and Engineering. An Introduction, John Wiley & Sons, Inc, New York, 2007
9. C. B. Carter, M. G. Norton, Ceramic Materials Science and Engineering, Springer-Verlag, Berlin-NewYork, 2007
10. C. Feldmann, T. Justel, C. R. Ronda, P. Schmidt, *Adv. Funct. Mater*. 13 (2003) 511-516
15. G. Blasse, A. Brill, *J. Lumin*. 3 (1970) 109-131
16. G. Blasse, *J. Solid State Chem.* 7 (1973) 169-171
41. G. Blasse, M. J. J. Lammers, H. C. G. Verhaar, L. H. Brixner, C. C. Torardi, *J. Solid State Chem*. 60 (1985) 258-261
42. G. Blasse, L. H. Brixner, *J. Solid State Chem.* 82 (1989) 151-155
43. G. Blasse, L. H. Brixner, *Chem. Phys. Lett.* 173 (1990) 409-411
44. L. H. Brixner, G. Blasse, *J. Phys. Chem. Solids* 52 (1991) 623-627
45. W. J. Schipper, M. F. Hoogendorp, G. Blasse, *J. Alloys Comp*. 202 (1993) 283-287
22. L. H. Brixner, *X-ray intensifying screen based on rare earth tantalate* US Pat. 4225653, 1980
23. L. H. Brixner, H. Y. Chen, *J. Electrochem. Soc.* 130 (1983) 2435-2443
24. H. J. Rossel, *J. Solid State Chem*. 27 (1979) 287-292
25. H. J. Rossel, *J. Solid State Chem*. 27 (1979) 115-122
26. D. Hedden, C. Torardi, W. Zegarski, *J. Solid State Chem.* 118 (1995) 419-421
28. S. A. Mather, P. K. Davies, *J. Am. Ceram. Soc*. 78 (1995) 2737-2745
30. G. M. Wolten, *Acta Crystallogr*. 23 (1967) 939-944
31. G. M. Wolten, A. B. Chase, *Am. Mineralogist* 52 (1967) 1536-1541
32. L. N. Lykova, N. S. Afonskii, *Russian J. Inorg. Chem*. 14 (1969) 742-743
33. V. S. Vasilev, M. M. Pinaeva, S. F. Shkirman, *Russian J. Inorg. Chem.* 24 (1979) 578-582
34. J. Graham, M. R. Thornber, *Am. Mineralogist*, 59 (1974) 1026-1039
35. J. Graham, M. R. Thornber, *Am. Mineralogist* 59 (1974) 1047-1050
36. W. W. Barker, J. Graham, *Am. Mineralogist* 59 (1974) 1051-1054
37. G. Blasse, L. H. Brixner, *J. Solid State Chem.* 82 (1989) 151-155
38. Y. Yokogama, M. Yoshimura, *J. Am. Ceram. Soc*. 74 (1991) 2077-2081
39. N. A. Bondar, A. I. Kalinin, L. L. Koroleva *Inorg. Mater.* 8 (1972) 1649-1650
40. I. D. Arellano, M. Nazarov, D. Y. Noh, *Rev. Columbiana de Fisica* 41 (2009) 123-127
48. B. Li, Z. Gu, J. Lin, M. Z. Su, *Mat. Research Bull.* 35 (2000) 1921-1931
50. L. Bo, Z. N. Gu, J. H. Lin, M. Z. Su, *Chem. J. Chinese Univ*. 22 (2001) 1-5
51. B. Li, Z. Gu, J. Lin, M. Z. Su, *J. Mat. Science* 35 (2000) 1139-1143

52. A. M. G. Massabni, G. J. M. Montandon, M. A. C. Santos, *Materials Research* 1 (1998) 1-4
53. S. H. Shin, D. Y. Jeon, *J. Appl. Phys.* 90 (2001) 5986-5990
54. L. H. Brixner, *Inorg. Chimica Acta* 140 (1987) 97-100
55. M. H. Hwang, Y. J. Kim, *Ceramics International* 34 (2008) 1117-1120
59. E. J. Popovici, F. Imre-Lucaci, L. Muresan, M. Stefan, E. Bica, R. Grecu, E. Indrea *J. Optoelectron. Adv. Mat.* 10 (2008) 2334 – 2337
63. C. B. Carter, M. G. Norton, Ceramic Materials – Science and Engineering, Springer Science –Business Media, New York, 2007

Chapter 6:

10. M. S. Bhuian, M. Paranthaman, K. Salama, *Supercond. Sci. Technol*. 19 (2006) R1-R21
11. M. S. Bhuian, M. Paranthaman, S. Sarhyamurthy, *J. Electronic Mat.* 36 (2007) 1270-1274
12. A. Llordes, K. Zalamova, S. Ricart, A. Palau, A. Pomar, T. Puig, A. Hardy, M. K. Van Bael, X. Obradors, *Chem Mat.* 22 (2010) 1686-1694
13. T. Araki, I. Hirabayashi, *Supercond. Sci. Technol*. 16 (2003) R71-R94
14 W. D. Callister, Jr. – Materials Science and Engineering. An Introduction, John Wiley & Sons, Inc, New York, 2007
15. G. Blasse, *J. Solid State Chem.* 7 (1973) 169-171
16. E. J. Popovici, M. Nazarov, L. Muresan,D. Y. Noh, L. B. Tudoran, E. Bica, E. Indrea, *J. Alloys Comp.* 497 (2010) 201-209

PUBLISHED PAPERS

1. Yttrium tantalate – based phosphors for x-ray intensifying screen
   Amalia Hristea, Laura Muresan, Emil Indrea, Marilena Vasilescu and Elisabeth.–J. Popovici
   SPIE (Bellingham, USA) Proceeding Series, ROMOPTO 2003, 5581, **2004**, 781-787

2. Studie on the influence of flux nature on the properties of niobium activated yttrium tantalate phosphor
   Amalia Mesaroş, Elisabeth-Jeanne Popovici, Laura Muresan, Maria Stefan , Rodica Grecu and Marinela Vasilescu, Studia *Universitatis Babes-Bolyai, Chemia 2*, LI, **2006**, 135-140

3. Luminescent thin films of nanocrystalline $YTaO_4$:Nb by pulsed laser deposition
   Amalia Hristea, Oscar Alm, Elisabeth-Jeanne Popovici and Mats Boman,
   Thin Solid Films 516, **2008**, 8431-8435

4. Morpho-structural and luminescent investigations of niobium activated yttrium tantalate powders,
   Amalia Hristea, Elisabeth-Jeanne Popovici, Laura Muresan, Maria Stefan , Rodica Grecu, Anders Johansson and Mats Boman
   Journal of Alloys and Compunds 471, **2009**, 524-529